We would like to thank the reviewer for the constructive comments really helping to improve the paper. Below, we address each comment in full detail. Following the Reviewers' comments in black, please find our point-to-point responses in blue. Hereafter, all new added or modified sentences are marked in blue and italic in this response.

Anonymous Referee #2

I have some major concerns of using FDDA for a study like this and try to objectively learn from model performance. When using FDDA, nudging is forcing the model to the same observations that are being used for evaluation (NCEP reanalysis includes probably all observations that are using for evaluation). Additionally, FDDA makes conclusions for feedback studies very problematic, since the physics parameterizations react in very different ways. Furthermore, you are using different physics and chemistry routines in all models. This makes this an "apples to oranges" comparison. Do you know what happens in Morrison microphysics when the mix-activation routine is not called (no chemistry)? My first thought was to reject the paper, however, the authors have done an immense amount of work and present some useful results that can be used by some of the developers. In turn I will propose accepting but with major revisions. These major revisions should be focused on the interpretation of the results. Abstract and conclusions should clearly say that this work is NOT to decide which model is better or worse since employed setups are very different and furthermore, it is not clear how FDDA runs influences feedback studies. Also, the authors need to be clear on what is used by Radiation (R) and MicroPhysics (MP) if feedback is off versus on. Are you just using a constant droplet number? A climatology? WRF-Chem has a lot of options, how come you decided to use different physics than in WRF-CMAQ? Chimere is way behind in the WRF version used, which makes that one even harder to compare. I am not asking you to rerun this monster simulation, but you will need to rephrase some of your abstract, conclusion, and results description. Since this reviewer is not asking for additional runs, this should not be a major effort. I really appreciate the work you folks put into this paper!

It would be interesting, maybe in a later additional paper, to compare the feedbacks in the different models for a shorter run that does not use FDDA. Maybe picking one or several interesting 5 day periods from the long runs that you used for this paper.

To answer the major concerned questions brought by the reviewer about FDDA in the coupled models, we put our response into three parts:

Enabling FDDA can improve the accuracy of simulated meteorology, e.g., temperature, wind speed and precipitation (Otte et al., 2012; Sommerfeld et al., 2019; Wang et al., 2016; Huang et al., 2021), and air quality, e.g., $PM_{2.5}$, PM_{10}, and O_3 (Barna and Lamb, 2000; Otte, 2008a, 2008b; Jeon et al., 2015; Tran et al., 2018). Enabling FDDA in WRF is

to decrease the error accumulations and avoid the significant deviations between simulation and observation, it is particularly beneficial in dynamic analyses of long-term simulations of meteorology and air quality (Otte et al., 2008). In this study, the 6-hourly NCEP-FNL data were used in the FDDA nudging, and hourly evaluations were conducted. We set the nudging coefficients for u/v components, temperature and water vapor mixing ratio above the planetary boundary layer (PBL) as 0.0001, 0.0001 and 0.00001 s^{-1}, respectively. The nudging coefficients for surface u/v components, temperature and water vapor mixing ratio are set to 0. Since we mainly focused on surface variables in the most evaluations of this study, the considerations of FDDA have relative limited impacts on our evaluation results.

Until now, the impacts of enabling FDDA on aerosol feedback effects are still under debate:

(1) Previous studies pointed out that enabling FDDA can reduce the simulated effects of aerosol feedbacks. The impact of aerosol feedbacks is diminished when comparing two-way coupled models of WRF-Chem and WRF-CMAQ with enabling FDDA to those without enabling FDDA (Forkel et al., 2012; Hogrefe et al., 2015; Zhang et al., 2016), and suggested that future works should be achieved the optimal balance between enabling options of FFDA and aerosol feedbacks. In the perspective part of Wong et al. (2012), the authors also pointed that aerosol-radiation interaction (ARI) effects could be attenuated by enabling FDDA, depending on the strength of the nudging coefficients employed. Hogrefe et al. (2015) emphasized that it is difficult to identify the extent to which nudging may have diminished the impact of simulated aerosol feedback effects. Referring to the model setting experiences of long-term aerosol feedback simulations in Gan et al. (2015) and Xing et al. (2015), the nudging coefficients for u/v wind, temperature, and water vapor mixing ratio were set to 0.00005 s^{-1}, 0.00005 s^{-1}, and 0.00001 s^{-1}, respectively.

(2) Several researches have used the coupled models with FFDA nudging technology to investigate aerosol feedback effects at the regional scales. All nudging coefficients of u/v components, temperature and water vapor mixing ratio are set to 0.0003 s^{-1} above PBL (Sekiguchi et al., 2018). Nguyen et al., (2019a) adopted the nudging coefficients of u/v components and water vapor mixing ratio for 0.0001 s^{-1} in all layers, and nudging coefficients of temperature is set to 0.0001 s^{-1} above PBL. Another study only considered the nudging coefficients of u/v components in all vertical layers with 0.0001 s^{-1} and 0.0003 s^{-1} for domains D01 and D02, respectively (Nguyen et al., 2019b). The FDDA nudging technology was applied to better represent the realistic atmosphere.

In future, we will choose several 5-day heavy pollution episodes in our long-run simulations and conduct sensitive simulations by turning off FDDA. We further evaluate and quantify the difference of impacts of FDDA on aerosol feedbacks among different coupled models in another research paper.

To make this point clear to readers, we have added relevant information in the Section 2.1 and conclusion section as follows:

Lines 137-142: *"Turing on FDDA in two-way coupled models could dampen the simulated aerosol feedbacks (Wong et al., 2012; Forkel et al., 2012; Hogrefe et al., 2015; Zhang et al., 2016). To reduce the effects of enabling FDDA on aerosol feedbacks in long-term simulations, here the nudging coefficients for u/v wind, temperature, and water vapor mixing ratio above the planetary boundary layer were set to 0.0001 s^{-1}, 0.0001 s^{-1}, and 0.00001 s^{-1}, respectively."*

Lines 759-762: "*In addition, FDDA nudging technique can attenuate the ARI effects during severe air polluted episodes, and optimal nudging coefficients among different regions need to be determined.*"

2. You are using different physics and chemistry routines in all models. This makes this an "apples to oranges" comparison.

Response: As we have not clearly described the selection principles of physics and chemistry routines in the methodology part, which made the reviewer and readers to have the sense of "apples to oranges" comparison. To solve it, more explanations were added in Lines 228-230 of the revised manuscript as follows:

"*To compare simulations by three coupled models, the respective model configurations of physics and chemistry routines are set as consistent as possible.*"

In the result part, we further rewrote related subtitles and sentences on multi-model evaluation results, as follows:

Line 239: "Meteorological evaluations and intercomparisons" was revised as "Multi-model meteorological evaluations".

Lines 257-259: "The overall model performances of WRF-CMAQ and WRF-Chem were better than that of WRF-CHIMERE, while all simulated results were overestimated at both annual and seasonal scales (MBs in spring and summer were larger than those in autumn and winter)." was revised as "All simulated results were overestimated at both annual and seasonal scales (MBs in spring and summer were larger than those in autumn and winter)."

Line 516: "Air quality evaluations and intercomparisons" was revised as "Multi-model air quality evaluations".

Line 559-560: "For O_3, WRF-CHIMERE (R = 0.62) exhibited the best model performance, followed by WRF-CMAQ (R = 0.55), and WRF-Chem (R = 0.45) (Table 4 and Figure S15)." was revised as "For O_3, WRF-CHIMERE (R = 0.62) exhibited the

highest correlation, followed by WRF-CMAQ (R = 0.55), and WRF-Chem (R = 0.45) (Table 4 and Fig. S16)."

Line 647-649: "The simulation accuracies of NO_2 columns via WRF-CHIMERE were significantly better than those using WRF-CMAQ or WRF-Chem in all seasons except for winter (Figure S20)" was revised as "The seasonal NO_2 columns were generally underestimated in WRF-CMAQ (-0.68 to -0.16 DU), WRF-Chem (-1.40 to -0.44 DU), WRF-CHIMERE (-1.31 to -0.19 DU) (Fig. S22).".

3. Do you know what happens in Morrison microphysics when the mix-activation routine is not called (no chemistry)?

Response: Whether aerosol feedbacks are enabled in WRF-CMAQ and WRF-Chem or not, Morrison microphysics scheme calculate the number concentrations and mixing ratios of five hydrometeor species (cloud water, rain, ice, snow and graupel) including 26 microphysical processes as listed in Table R1 (Morrison et al., 2008). If the mix-activation routine is not called, cloud water mixing ratio is predicted and cloud droplet number concentration (CDNC) is prescribed as the constant value of 250 cm^{-3} (Yang et al., 2011). Then, cloud water and constant cloud droplet effective radius from Morrison scheme are used to drive RRTMG shortwave and longwave radiation schemes in coupled models.

With considering aerosol-cloud interactions, prognostic CDNC were online calculated in Morrison microphysics scheme based on Köhler theory. CDNC further alter cloud droplet effective radius (r_c), which is calculated in the RRTMG shortwave and longwave radiation schemes as follows.

$$r_c = \left(\frac{3L_c}{4\pi\rho_w N_c}\right)^{1/3} \quad (1)$$

where ρ_w denotes the cloud liquid water density, L_c and N_c are the cloud water mixing ratio and cloud droplet number concentration, respectively.

Once the r_c changes, the corresponding cloud optical parameters (cloud extinction coefficient (β_c), single scattering albedo (ω_c), and asymmetry factor (g_c)) also vary, and the empirical formulas are expressed as:

$$\beta_c = L_c(a_1 r_c^{b_1} + c_1) \quad (2)$$

$$\omega_c = 1-(a_2 r_c^{b_2} + c_2) \quad (3)$$

$$g_c = a_3 r_c^{b_3} + c_3 \quad (4)$$

where L_c stands for the cloud water mixing ratio, and a_i, b_i and c_i are the functions of wavelength (Hu and Stamnes, 1993).

Regarding the precipitation, the cloud-to-rain autoconversion rate (P) are calculated in the Morrison cloud microphysics scheme (Khairoutdinov and Kogan, 2000):

$$P = 1350 N_c^{-1.79} L_c^{2.47} \quad (5)$$

For the Thompson microphysics scheme in WRF-CHIMERE, the CDNC is set as a constant value of 300 cm^{-3} without considering aerosol feedbacks or only enabling ARI. With only enabling ACI or both ARI and ACI, the method for calculating prognostic CDNC in the Thompson scheme is the same as that in the Morrison scheme, but the discrepancies of representations for cloud droplet effective radius (Eqs. 1 and 6) and cloud-to-rain autoconversion rate (Eqs. 5 and 8) exist in these two schemes.

$$r_c=\left(\frac{3+\left(\frac{1000}{N_c}+2\right)}{2\lambda_c}\right) \tag{6}$$

$$\lambda_c=\begin{cases}\left(\frac{N_c\pi\times1000\times4896}{6L_c}\right)^{1/3} & \text{for } N_c \le 100,\\ \left(\frac{N_c\pi\times1000\times60}{6L_c}\right)^{1/3} & \text{for } N_c \ge 10^{10},\\ \left(\frac{N_c\pi\times1000\times g\_ratio[\min(15,(\frac{1000}{N_c}+2))]}{6L_c}\right)^{1/3} & \text{otherwise.}\end{cases} \tag{7}$$

where g_ratio is an array with values of 24, 60, 120, 210, 336, 504, 720, 990, 1320, 1716, 2184, 2730, 3360, 4080 and 4896.

Compared to the Morrison scheme, Thompson scheme has the capability to calculate the number concentration (N_i) of ice nucleating particles (INP), and detailed information is presented in Table S6 of Supplement of the revised manuscript. Similar to cloud droplet, N_i also has the impacts on cloud ice effective radius and further their optical properties (β_i, ω_i and g_i) as follows.

$$r_i=\left(\frac{3}{2\lambda_i}\right) \tag{8}$$

$$\lambda_i=\left(\frac{N_i\pi\times890\times\Gamma(4)}{6L_i\times\Gamma(1)}\right)^{1/3} \tag{9}$$

$$\beta_i=I_c\left(a_0+\frac{a_1}{r_i}\right) \tag{10}$$

$$\omega_i=1-(b_0+b_1r_e+b_2r_e^2+b_3r_e^3) \tag{11}$$

$$g_i=c_0+c_1r_e+c_2r_e^2+c_3r_e^3 \tag{12}$$

where β_i, ω_i and g_i are the ice extinction coefficient, single scattering albedo and asymmetry factor, respectively. I_c stands for the ice water content, a_i, b_i and c_i are the coefficient functions of wavelengths, and their detailed information are provided in the Tables 3a-d of Fu (1996).

The physical formulation for calculating cloud-to-rain autoconversion rate is adopted from Berry and Reinhardt (1974):

$$P=\frac{0.027\rho L_c\left(\frac{1}{16}\times10^{20}D_b^3D_f\text{-}0.4\right)}{\frac{3.72}{\rho L_c}\left(\frac{1}{2}\times10^6D_b\text{-}7.5\right)}^{-1} \tag{13}$$

$$D_f=\left(\frac{6\rho L_c}{\pi\rho_w N_c}\right)^{1/3} \tag{14}$$

$$D_g = \frac{\left[\frac{\Gamma(\mu_c+7)}{\Gamma(\mu_c+4)}\right]^{1/3}}{\lambda_c} \quad (15)$$

$$D_b = (D_f^3 D_g^3 - D_f^6)^{1/6} \quad (16)$$

where ρ is the moist air density, ρ_w is the cloud liquid water density, D_b, D_g and D_f are the characteristic diameters, μ_c and λ_c are the shape and slope parameters of gramma size distribution (Γ), respectively.

Table R1 Summary of microphysical process in the Morrison scheme

No.	Process name
1	Ice nucleation from freezing of aerosol
2	Droplet activation from aerosol
3	Ice multiplication
4	Autoconversion of droplets to from rain
5	Autoconversion of ice to form snow
6	Accretion of droplets by rain
7	Accretion of droplets by snow
8	Accretion of rain by snow
9	Accretion of cloud ice by snow
10	Heterogeneous freezing of droplets to form cloud ice
11	Heterogeneous freezing of rain to form snow
12	Melting of snow to form rain
13	Melting of cloud ice to form droplets
14	Self-collection of droplets
15	Self-collection of cloud ice
16	Self-collection of snow
17	Self-collection of rain
18	Loss of N due to sublimation of cloud ice
19	Loss of N due to evaporation of rain
20	Loss of N due to sublimation of snow
21	Deposition/sublimation of cloud ice
22	Condensation/evaporation of droplets
23	Condensation/evaporation of rain
24	Deposition/sublimation of snow
25	Homogeneous freezing of droplets to form cloud ice
26	Homogeneous freezing of rain to form snow

4. The authors need to be clear on what is used by Radiation (R) and MicroPhysics (MP) if feedback is off versus on.

Response: In the two-way coupled models, for the radiation calculation processes, numerous combinations of radiation and microphysics schemes are presented, and our selections in this study are presented in Figure S26.

When aerosol feedback is turned on, for radiation, the spectral optical properties of different aerosol species groups and heating rates (ttenld) are online calculated, and then inter/extrapolated into specific shortwave (SW) and longwave (LW) bands in the RRTMG SW/LW schemes (Tables S5–S6). For microphysics, when the ACI feedback is turned on, the prognostic cloud droplet number concentration (CDNC) or/and ice nucleating particle concentration (INP), optical properties of cloud liquid water and ice is taken into account in the Morrison scheme of WRF-Chem and Thompson scheme of WRF-CHIMERE (Table S7).

When aerosol feedback is turned off, for radiation, the option of aer_opt is set to 0 (no aerosols) as baseline scenario in our study, which result in no calculations of aerosol optical properties in RRTMG, as shown in Table S6. Although aer_opt=1 or 2 can be set when feedback is off (the climatology data or empirical formulas of aerosol optical properties were utilized to calculate aerosol radiative effects), the corresponding simulated results can not be used as baseline scenario to quantify the ARI effects in our study. For microphysics, prescribed CDNC are set to 250 and 300 cm^{-3} in the Morrison scheme of WRF-Chem and Thompson scheme of WRF-CHIMERE WRF-Chem and WRF-CHIMERE, respectively. The prescribed INP are calculated by the empirical formula of temperature in these three coupled models (Rasmussen et al., 2002; DeMott et al., 2015; Thompson and Eidhammer, 2014).

To reflect the above information, we compiled the Tables S6-S8 and plotted the Figure S24 and put them into the Supplement of the revised manuscript. We also added the sentences in the revised manuscript as follows.

Lines 408-422: "*When ARI effects are enabled, the diversities of refractive indices of aerosol species groups lead to the discrepancies of online calculated aerosol optical properties in different shortwave and longwave (SW and LW) bands in the RRTMG SW/LW radiation schemes of WRF-CMAQ, WRF-Chem, and WRF-CHIMERE (Tables S5–S6). The online calculated cloud optical properties induced by aerosol absorption in the RRTMG radiation schemes are different in treatments of aerosol species groups in the three coupled models. With enabling ACI effects, the activation of cloud droplets from aerosols based on the Köhler theory is taken into account in WRF-Chem and WRF-CHIMERE, in comparison to simulations without aerosol feedbacks (Table S7). The treatments of prognostic ice nucleating particles (INP) formed via heterogeneous nucleation of dust particles (diameters > 0.5 μm) and homogeneous freezing of hygroscopic aerosols (diameters > 0.1 μm) are only considered in WRF-CHIMERE, but the prognostic ice nucleating particles are not included in WRF-CMAQ and WRF-Chem. These discrepancies eventually contribute to the differences of simulated radiation changes caused by aerosols.*"

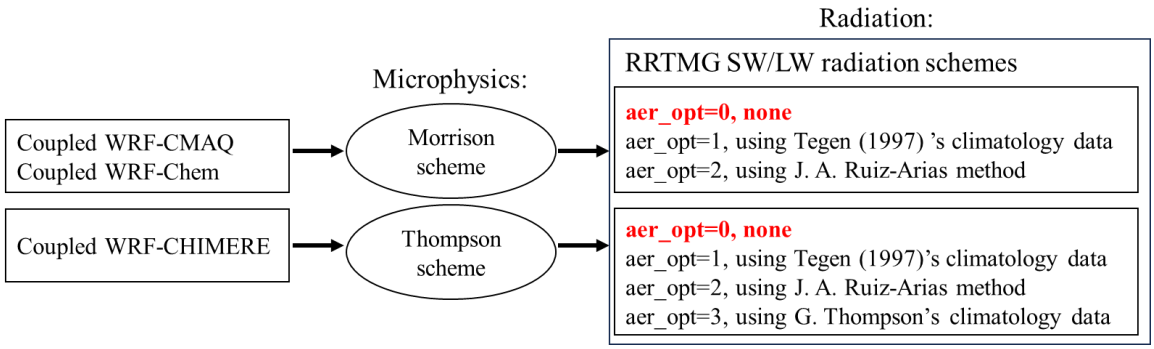

Figure S26. Summary of the selected options of radiation and microphysics schemes in coupled WRF-CMAQ, WRF-Chem and WRF-CHIMERE in this study.

Table S5. Radiation variables used in the two-way coupled WRF-CMAQ, WRF-Chem and WRF-CHIMERE models with only enabling ARI compared to without aerosol feedbacks.

Model	*SW/LW radiation schemes*	*Turning off feedback*	*Turning on ARI feedback*	
			Direct effects	*Semi-direct effects*
WRF-CMAQ	*RRTMG/RRTMG*	*Aerosol optical properties are not calculated*	*Aerosol extinction, single scattering albedo (ω_o), and asymmetry factor (g) 14 shortwave bands and 5 longwave bands (Wong et al., 2012)*	*1. Solar uv and ir fluxes 2. Radiative heating rate for the tten1d variable*
WRF-Chem	*RRTMG/RRTMG*	*Aerosol optical properties are not calculated*	*ω_o (300 nm, 400 nm, 600 nm, 999 nm), g (300 nm, 400 nm, 600 nm, 999 nm), AOD (τ) (300 nm, 400 nm, 600 nm, 999 nm, 16 bands 3400 nm to 55600 nm) (Zhao et al., 2011)*	*1. Solar uv and ir fluxes 2. Radiative heating rate for the tten1d variable*
WRF-CHIMERE	*RRTMG/RRTMG*	*Aerosol optical properties are not calculated*	*ω_o (400 nm, 600 nm), g (400 nm, 600 nm), AOD (300 nm, 400 nm, 999 nm, 16 bands 3400 nm to 55600 nm) (Briant et al., 2017)*	*1. Solar uv and ir fluxes 2. Radiative heating rate for the tten1d variable*

Table S6. Description of refractive indices and radiation schemes used in the WRF-CMAQ, WRF-Chem and WRF-CHIMERE models.

Model	*Refractive indices of aerosol species groups*	
	SW	*LW*
WRF-CMAQ	*1. Water (1.408+1.420×10^{-2}i, 1.324+1.577×10^{-4}i, 1.277+1.516×10^{-3}i, 1.302+1.159×10^{-3}i, 1.312+2.360×10^{-4}i, 1.321+1.713×10^{-4}i, 1.323+2.425×10^{-5}i, 1.327+3.125×10^{-6}i, 1.331+3.405×10^{-8}i, 1.334+1.639×10^{-9}i, 1.340+2.955×10^{-9}i, 1.349+1.635×10^{-8}i, 1.362+3.350×10^{-8}i, 1.260+6.220×10^{-2}i) 2. Water-soluble (1.443+5.718×10^{-3}i, 1.420+1.777×10^{-2}i, 1.420+1.060×10^{-2}i, 1.420+8.368×10^{-3}i, 1.463+1.621×10^{-2}i, 1.510+2.198×10^{-2}i, 1.510+1.929×10^{-2}i, 1.520+1.564×10^{-2}i, 1.530+7.000×10^{-3}i, 1.530+5.666×10^{-3}i, 1.530+5.000×10^{-3}i, 1.530+8.440×10^{-3}i, 1.530+3.000×10^{-2}i, 1.710+1.100×10^{-1}i) 3. BC (2.089+1.070i, 2.014+0.939i, 1.962+0.843i, 1.950+0.784i, 1.940+0.760i, 1.930+0.749i, 1.905+0.737i, 1.870+0.726i, 1.850+0.710i, 1.850+0.710i, 1.850+0.710i, 1.850+0.710i, 1.850+0.710i, 2.589+1.771i) 4. Insoluble (1.272+1.165×10^{-2}i, 1.168+1.073×10^{-2}i, 1.208+8.650×10^{-3}i, 1.253+8.092×10^{-3}i, 1.329+8.000×10^{-3}i, 1.418+8.000×10^{-3}i, 1.456+8.000×10^{-3}i, 1.518+8.000×10^{-3}i, 1.530+8.000×10^{-3}i, 1.530+8.000×10^{-3}i, 1.530+8.000×10^{-3}i, 1.530+8.440×10^{-3}i, 1.530+3.000×10^{-2}i, 1.470+9.000×10^{-2}i) 5. Sea-salt (1.480+1.758×10^{-3}i, 1.534+7.462×10^{-3}i, 1.437+2.950×10^{-3}i, 1.448+1.276×10^{-3}i, 1.450+7.944×10^{-4}i, 1.462+5.382×10^{-4}i, 1.469+3.754×10^{-4}i, 1.470+1.498×10^{-4}i, 1.490+2.050×10^{-7}i, 1.500+1.184×10^{-6}i, 1.502+9.938×10^{-6}i, 1.510+2.060×10^{-6}i, 1.510+5.000×10^{-6}i, 1.510+1.000×10^{-2}i) in term of 14 wavelengths at 3.4615, 2.7885, 2.325, 2.046, 1.784, 1.4625, 1.2705, 1.0101, 0.7016, 0.53325, 0.38815, 0.299, 0.2316, 8.24 μm*	*1. Water (1.160+0.321i, 1.140+0.117i, 1.232+0.047i, 1.266+0.038i, 1.300+0.034i) 2. Water-soluble (1.570+0.069i, 1.700+0.055i, 1.890+0.128i, 2.233+0.334i, 1.220+0.066i) 3. BC (1.570+2.200i, 1.700+2.200i, 1.890+2.200i, 2.233+2.200i, 1.220+2.200i) 4. Insoluble (1.482+0.096i, 1.600+0.107i, 1.739+0.162i, 1.508+0.117i, 1.175+0.042i) 5. Sea-salt (1.410+0.019i, 1.490+0.014i, 1.560+0.017i, 1.600+0.029i, 1.402+0.012i) in term of 5 thermal windows at 13.240, 11.20, 9.73, 8.870, 7.830 μm*
WRF-Chem	*1. Water (1.35+1.524×10^{-8}i, 1.34+2.494×10^{-8}i, 1.33+1.638×10^{-8}i, 1.33+3.128×10^{-6}i) 2. Dust (1.55+0.003i, 1.550+0.003i, 1.550+0.003i, 1.550+0.003i) 3. BC (1.95+0.79i, 1.95+0.79i, 1.95+0.79i, 1.95+0.79i) 4. OC (1.45+0i, 1.45+0i, 1.45+0i, 1.45+0i) 5. Sea salt (1.51+8.66×10^{-7}i, 1.5+7.019×10^{-8}i, 1.5+1.184×10^{-5}i, 1.47+1.5×10^{-4}i) 6. Sulfate (1.52+1.00×10^{-8}i, 1.52+1.00×10^{-8}i, 1.52+1.00×10^{-8}i, 1.52+1.75×10^{-6}i) in term of 4 spectral intervals in 0.25-0.35, 0.35-0.45, 0.55-0.65, 0.998-1.000 μm*	*1. Water (1.532+0.336i, 1.524+0.360i, 1.420+0.426i, 1.274+0.403i, 1.161+0.321i, 1.142+0.115i, 1.232+0.047i, 1.266+0.039i, 1.296+0.034i, 1.321+0.0344i, 1.342+0.092i, 1.315+0.012i, 1.330+0.013i, 1.339+0.01i, 1.350+0.0049i, 1.408+0.0142i) 2. Dust (2.34+0.7i, 2.904+0.857i, 1.748+0.462i, 1.508+0.263i, 1.911+0.319i, 1.822+0.26i, 2.917+0.65i, 1.557+0.373i, 1.242+0.093i, 1.447+0.105i, 1.432+0.061i, 1.473+0.0245i, 1.495+0.011i, 1.5+0.008i) 3. BC (1.95+0.79i, 1.95+0.79i, 1.95+0.79i, 1.95+0.79i, 1.95+0.79i, 1.95+0.79i, 1.95+0.79i, 1.95+0.79i, 1.95+0.79i, 1.95+0.79i, 1.95+0.79i, 1.95+0.79i, 1.95+0.79i, 1.95+0.79i,) 4. OC (1.86+0.5i, 1.91+0.268i, 1.988+0.185i, 1.439+0.198i, 1.606+0.059i, 1.7+0.0488i, 1.888+0.11i, 2.489+0.3345i, 1.219+0.065i, 1.419+0.058i, 1.426+0.0261i, 1.446+0.0142i, 1.457+0.013i, 1.458+0.01i) 5. Sea salt (1.74+0.1978i, 1.76+0.1978i, 1.78+0.129i, 1.456+0.038i, 1.41+0.019i, 1.48+0.014i, 1.56+0.016i, 1.63+0.03i, 1.4+0.012i, 1.43+0.0064i, 1.56+0.0196i, 1.45+0.0029i, 1.485+0.0017i, 1.486+0.0014i) 6. Sulfate (1.89+0.22i, 1.91+0.152i, 1.93+0.0846i, 1.586+0.2225i, 1.678+0.195i, 1.758+0.441i, 1.855+0.696i, 1.597+0.695i, 1.15+0.459i, 1.26+0.161i, 1.42+0.172i, 1.35+0.14i, 1.379+0.12i, 1.385+0.122i) in term of 16 spectral intervals in 10-350, 350-500, 500-630, 630-700, 700-820,*

WRF-CHIMERE	*1. Water (1.35+2.0×10⁻⁸i, 1.34+2.0×10⁻⁸i, 1.34+1.8×10⁻⁸i, 1.33+3.4×10⁻⁸i, 1.33+3.9×10⁻⁷i)* *2. Dust (1.53+0.0055i, 1.53+0.0055i, 1.53+0.0024i, 1.53+8.9-4i, 1.53+7.6-4i)* *3. BC (1.95+0.79i, 1.95+0.79i, 1.95+0.79i, 1.95+0.79i, 1.95+0.79i)* *4. OC (1.53+0.09i, 1.53+0.008i, 1.53+0.005i, 1.53+0.0063i, 1.52+0.016i)* *5. Sea salt (1.38+8.7×10⁻⁷i, 1.38+3.5×10⁻⁷i, 1.37+6.6×10⁻⁹i, 1.36+1.2×10⁻⁸i, 1.35+2.6×10⁻⁵i)* *6. PPM (1.53+0.008i, 1.52+0.008i, 1.52+0.008i, 1.51+0.008i, 1.5+0.008i)* *7. SOA (1.56+0.003i, 1.56+0.003i, 1.56+0.003i, 1.56+0.003i, 1.56+0.003i)* *8. H_2SO_4 (1.5+1.0×10⁻⁸i, 1.47+1.0×10⁻⁸i, 1.44+1.0×10⁻⁸i, 1.43+1.3×10⁻⁸i, 1.42+1.2×10⁻⁶i)* *9. HNO_3 (1.53+0.006i, 1.53+0.006i, 1.53+0.006i, 1.53+0.006i, 1.53+0.006i)* *10. NH_3 (1.53+0.0005i, 1.52+0.0005i, 1.52+0.0005i, 1.52+0.0005i, 1.52+0.0005i) in term of 5 wavelengths at 0.2, 0.3, 0.4, 0.6, 0.999 μm*	*820-980, 980-1080, 1080-1180, 1180-1390, 1390-1480, 1480-1800, 1800-2080, 2080-2250, 2250-2390, 2390-2600, 2600-3250 cm⁻¹* *1. Water (1.42+0.02i, 1.35+0.0047i, 1.34+0.0085i, 1.33+0.015i, 1.32+0.01i, 1.32+0.13i, 1.32+0.032i, 1.3+0.034i, 1.27+0.039i, 1.23+0.047i, 1.15+0.1i, 1.16+0.32i, 1.27+0.4i, 1.41+0.43i, 1.52+0.37i, 1.65+0.55i)* *2. BC (1.95+0.79i, 1.95+0.79i, 1.95+0.79i, 1.95+0.79i, 1.95+0.79i, 1.95+0.79i, 1.95+0.79i, 1.95+0.79i, 1.95+0.79i, 1.95+0.79i, 1.95+0.79i, 1.95+0.79i, 1.95+0.79i, 1.95+0.79i, 1.95+0.79i, 1.95+0.79i)* *3. OC (1.43+1.42i, 1.46+1.43i, 1.46+1.25i, 1.46+2.67i, 1.45+1.89i, 1.42+1.71i, 1.43+1.71i, 1.25+0.007i, 2.67+0.005i, 1.89+0.01i, 1.71+0.013i, 1.43+0.014i, 1.46+0.025i, 1.46+0.062i, 1.46+0.064i, 1.45+0.031i)* *4. Salt (1.43+0.019i, 1.37+0.0043i, 1.36+0.0084i, 1.36+0.011i, 1.34+0.01i, 1.35+0.083i, 1.34+0.029i, 1.31+0.03i, 1.33+0.037i, 1.29+0.042i, 1.2+0.09i, 1.2+0.27i, 1.3+0.34i, 1.47+0.37i, 1.56+0.03i, 1.51+0.09i)* *5. PPM (1.45+0.01i, 1.45+0.01i, 1.45+0.01i, 1.45+0.01i, 1.45+0.01i, 1.45+0.01i, 1.45+0.05i, 1+0.5i, 1+0.2i, 2.6+0.2i, 1.7+0.2i, 1.7+0.2i, 1.7+0.2i, 1.7+0.2i, 1.7+0.2i, 1.7+0.2i)* *6. SOA (1.56+0.003i, 1.56+0.003i, 1.56+0.003i, 1.56+0.003i, 1.56+0.003i, 1.56+0.003i, 1.56+0.003i, 1.56+0.003i, 1.56+0.003i, 1.56+0.003i, 1.56+0.003i, 1.56+0.003i, 1.56+0.003i, 1.56+0.003i, 1.56+0.003i, 1.56+0.003i)* *7. H_2SO_4 (1.35+0.16i, 1.4+0.13i, 1.39+0.12i, 1.38+0.12i, 1.35+0.15i, 1.42+0.18i, 1.26+0.16i, 1.15+0.44i, 1.57+0.73i, 1.83+0.7i, 1.71+0.46i, 1.68+0.2i, 1.59+0.21i, 1.87+0.48i, 1.89+0.27i, 1.86+0.31i)* *8. HNO_3 (1.45+0.01i, 1.45+0.01i, 1.45+0.01i, 1.45+0.01i, 1.45+0.01i, 1.45+0.01i, 1.45+0.05i, 1+0.5i, 1+0.2i, 2.6+0.2i, 1.7+0.2i, 1.7+0.2i, 1.7+0.2i, 1.7+0.2i, 1.7+0.2i, 1.7+0.2i)* *9. NH_3 (1.45+0.01i, 1.45+0.01i, 1.45+0.01i, 1.45+0.01i, 1.45+0.01i, 1.45+0.01i, 1.45+0.05i, 1+0.5i, 1+0.2i, 2.6+0.2i, 1.7+0.2i, 1.7+0.2i, 1.7+0.2i, 1.7+0.2i, 1.7+0.2i, 1.7+0.2i) in term of 16 wavelengths at 3.4, 4, 4.3, 4.6, 5.2, 6.1, 7.0, 7.8, 8.8, 9.7, 11.1, 13.2, 15.0, 17.7, 23.5, 55.6 μm*

Table S7. Microphysics variables used in the two-way coupled WRF-CMAQ, WRF-Chem and WRF-CHIMERE models with enabling ACI effects compared to without aerosol feedbacks.

Model	*Microphysics scheme*	*Turning off feedback*	*Turning on ACI feedback*	
			First indirect effects	*Second indirect effects*
WRF-CMAQ	*Morrison*	*1. Prescribed constant CDNC value of 250 cm^{-3}*	*None*	*None*
WRF-Chem	*Morrison*	*1. Prescribed constant CDNC value of 250 cm^{-3}* *2. Constant cloud droplet effective radius with 10 μm* *3. Cloud droplet extinction coefficient, single scattering albedo, and asymmetry factor based on Eqs. (2)-(4)* *4. Prescribed ice nucleating particle (INP) concentration based on empirical formula (Rasmussen et al., 2002)*	*1. Hygroscopicity* *2. Prognostic CDNC based on Köhler theory* *3. Prognostic cloud droplet effective radius* *4. Prognostic cloud droplet extinction coefficient, single scattering albedo, and asymmetry factor* *5. Prescribed INP*	*1. Prognostic cloud-to-rain autoconversion rate*
WRF-CHIMERE	*Thompson*	*1. Prescribed constant CDNC values of 300 cm^{-3}* *2. Prescribed INP from heterogeneous ice nucleation using climatical dust concentration (dimeters > 0.5μm) (DeMott et al., 2015) and homogeneous freezing (Thompson and Eidhammer, 2014) with climatological hygroscopic aerosol concentrations (dimeters > 0.1μm) generated by QNWFA_QNIFA_Monthly_GFS file* *3. Prescribed cloud droplet and ice effective radius* *4. Prescribed extinction coefficient, single scattering albedo, and asymmetry factor of cloud droplet and ice*	*1. Hygroscopicity* *2. Prognostic CDNC based on Köhler theory* *3. Prognostic INP from heterogeneous ice nucleation based on online dust calculation (dimeters > 0.5 μm) and homogeneous freezing with prognostic hygroscopic aerosol concentrations (dimeters > 0.1μm) (Tuccella et al., 2019)* *4. Prognostic cloud droplet and ice effective radius* *5. Prognostic extinction coefficient, single scattering albedo, and asymmetry factor of cloud droplet and ice*	*1. Prognostic cloud-to-rain autoconversion rate*

5. Are you just using a constant droplet number? A climatology?

Response: It depends on the situation. Without turning on aerosol feedbacks or only considering ARI, cloud droplet number concentration (CDNC) is prescribed as a constant value of 250 cm^{-3} in the Morrison scheme of WRF-CMAQ and WRF-Chem and 300 cm^{-3} in the Thompson scheme of WRF-CHIMERE. With enabling ACI or both ARI and ACI, the online calculation of (CDNC) is performed in WRF-Chem and WRF-CHIMERE by utilizing the aerosol activation parameterization (Abdul-Razzak and Ghan, 2002; Chapman et al., 2009; Tuccella et al., 2019).

The above information is added in Lines 486-496 of the revised manuscript as follows:

"*This may be explained as the different parameterization treatments of cloud droplet number concentration (CDNC) simulated by the three coupled models with/without enabling ACI effects. The cloud condensation nuclei activated from aerosol particles can increase CDNC and impact on LWP and CF. Without enabling any aerosol feedbacks or only enabling ARI, the CDNC is default prescribed as a constant value of 250 cm^{-3} in the Morrison scheme of WRF-CMAQ and WRF-Chem and 300 cm^{-3} in the Thompson scheme of WRF-CHIMERE. When only ACI or both ARI and ACI are enabled, the online calculating of prognostic CDNC is performed in WRF-Chem and WRF-CHIMERE by using the method of maximum supersaturation (Abdul-Razzak and Ghan, 2002; Chapman et al., 2009; Tuccella et al., 2019).*"

6. WRF-Chem has a lot of options, how come you decided to use different physics than in WRF-CMAQ?

Response: The options of commonly used physics schemes for the two-way coupled WRF-CMAQ and WRF-Chem models are summarized in the Table S1 of Gao et al. (2022). To keep the consistency of physical schemes, the same RRTMG shortwave and longwave radiation schemes and the Morrison microphysics scheme were adopted both in WRF-Chem and WRF-CMAQ. It should be noted that the microphysics processes only support the Thompson scheme in coupled WRF-CHIMERE. As possible as we can, the different cumulus, surface, and land surface schemes in WRF-CMAQ and WRF-Chem were chosen according to widely used options outlined in Table S1 of Gao et al. (2022). Related information is added in Section 2.1 of the revised manuscript as follows.

"*To keep the consistency of physical schemes, the same RRTMG shortwave and longwave radiation schemes and Morrison microphysics schemes are adopted in both WRF-Chem and WRF-CMAQ. WRF-CHIMERE applied the same radiation schemes and Thompson microphysics scheme. The different other schemes (cumulus, surface, and land surface) in WRF-CMAQ and WRF-Chem were chosen according to widely used options outlined in Table S1 of Gao et al. (2022). The other schemes used in WRF-CHIMERE are the same as with WRF-Chem.*"

Reference:

Gao C, Xiu A, Zhang X, et al. Two-way coupled meteorology and air quality models in Asia: a systematic review and meta-analysis of impacts of aerosol feedbacks on meteorology and air quality[J]. Atmospheric Chemistry and Physics, 2022, 22(8): 5265-5329.

7. Chimere is way behind in the WRF version used, which makes that one even harder to compare?

Response: Yes, it really makes the comparison to be harder. Even under the same setting of scientific options in namelist, different versions of WRF have notable impacts on the simulated results (Appel et al., 2021). Until now, the coupled WRF-CHIMERE only support the version 3.7.1 of WRF (Briant et al., 2017; Tuccella et al., 2019). In order to include this new developed coupled model into our inter-comparisons, we have to accept the lower version of WRF. To clarify this discrepancy, we added a new sentence in Lines 116-118 of the methodology part of the revised manuscript as follows.

"*Compared to WRF v4.1.1-CMAQ v5.3.1 and WRF-Chem v4.1.1, the coupled WRF-CHIMERE only support the version 3.7.1 of WRF (Briant et al., 2017; Tuccella et al., 2019).*"

8. I am not asking you to rerun this monster simulation, but you will need to rephrase some of your abstract, conclusion, and results description.

Response: Thanks for your suggestions, we have rewritten and modified some parts of the abstract, results and conclusion, and relevant revisions are as follows:

Abstract:

In the eastern China region, two-way coupled meteorology and air quality models have been applied aiming to more realistically simulate meteorology and air quality by accounting for the aerosol–radiation–cloud interactions. There have been numerous related studies being conducted, but the performances of multiple two-way coupled models simulating meteorology and air quality have not been compared in this region. In this study, we systematically evaluated annual and seasonal meteorological and air quality variables simulated by three open-source and widely used two-way coupled models (i.e., WRF-CMAQ, WRF-Chem, and WRF-CHIMERE) by validating the model results with surface and satellite observations for eastern China during 2017. Note that although we have done our best to keep the same configurations, this study is not aiming to screen which model is better or worse since different setups are still presented in simulations. Our evaluation results showed that all three two-way coupled models reasonably well simulated the annual spatiotemporal distributions of meteorological and air quality variables. The impacts of aerosol-cloud interaction (ACI) on model performances' improvements were limited compared to aerosol-radiation interaction (ARI), and several possible improvements on ACI representations in two-way coupled models are further discussed and proposed. When sufficient computational resources become available, two-way coupled models should be applied for more accurate air quality forecast and timely warning of heavy air pollution events in atmospheric environmental management. The potential improvements of two-way coupled models are proposed in future research perspectives.

Conclusions:

Applications of two-way coupled meteorology and air quality models have been performed in eastern China in recent years, but no research focused on the comprehensive assessments of multiple coupled models in this region. To the best of our knowledge, this is the first time to conduct comprehensive inter-comparisons among the open-sourced two-way coupled meteorology and air quality models (WRF-CMAQ, WRF-Chem, and WRF-CHIMERE). This study systemically evaluated the hindcast simulations for 2017 and explored the impacts of ARI and/or ACI on model and computational performances in eastern China.

After detailed comparisons with ground-based and satellite-borne observations, the evaluation results showed that three coupled models perform well for meteorology and air quality, especially for surface temperature (with R up to 0.97) and $PM_{2.5}$ concentrations (with R up to 0.68). The effects of aerosol feedbacks on model performances varied depending on the two-way coupled models, variables, and time scales. There were around 20%–70% increase of computational time when these two-way coupled models enabled aerosol feedbacks against simulations without aerosol-radiation-cloud interactions. It is noteworthy that all three coupled models could well reproduce the spatiotemporal distributions of satellite-retrieved CO column concentrations but not for ground-observed CO concentrations.

With inter-comparisons, some uncertainty sources can be ascertained in evaluating aerosol feedback effects. As numerous schemes can be combined in configurations of different coupled models, here we only evaluated simulations with specific settings. Future comparison works with considering more combinations of multiple schemes within the same or different coupled models need to be conducted. Among the three coupled models, the numerical representations for specific variable in same scheme are diverse, e.g., treatments of cloud cover and cloud optical properties in the Fast-JX photolysis scheme. More accurate representations of photolysis processes should be taken into account to reduce the evaluation uncertainties. In addition, FDDA nudging technique can attenuate the ARI effects during severe air polluted episodes, and optimal nudging coefficients among different regions need to be determined. Last but not least, the actual mechanisms underlying ACI effects are still unclear, and the new advances in the measurements and parameterizations of CCN/IN activations and precipitation need to be timely incorporated in coupled models.

Revisions of the result descriptions are as follows.

Lines 408-411: "*that the differences of aerosol representations contributed to the diversity of seasonal MBs. For example, 3 modes AERO6, 4 bins sectional MOSAIC and 10 bins SAM were implemented in WRF-CMAQ, WRF-Chem and WRF-CHIMERE, respectively (Table 2).*" is added.

Lines 415-429: "*The refractive indices of aerosol species groups show discrepancies for calculating aerosol optical depth or extinction coefficients, single scattering albedo and asymmetry factor in different shortwave and longwave (SW and LW) bands in RRTMG SW/LW radiation schemes of WRF-CMAQ, WRF-Chem, and WRF-CHIMERE when ARI effects are enabled (Tables S4 and S5). Representations of cloud optical depth induced by influence of various aerosol absorption of sunlight for the same RRTMG radiation schemes have the different attributing to treatments of aerosol in the three coupled models. The activation of cloud droplets from aerosols based on the Köhler theory is taken into account in the WRF-Chem and WRF-CHIMERE models with enabled ACI effects, in comparison to simulations without aerosol feedbacks (Table S6). However, parametrizations for ice nucleating (INP) formed via heterogeneous nucleation of (diameters > 0.5 μm) and homogeneous freezing of hygroscopic aerosols (diameters > 0.1 μm) are only implemented in WRF-CHIMERE. The descriptions of all radiation and cloud microphysics variables used in the three coupled models with enabling ARI or ACI effects compared to without enabling aerosol feedbacks are presented in Figure S23. These discrepancies result in a variety of simulated radiation changes caused by aerosol.*" is added.

Lines 498-507: "*This may be caused by the different treatments of cloud droplet number concentration (CDNC) resulting from the enabling or disabling ACI effects in coupled models. The cloud condensation nuclei activated from aerosol can increase CDNC and affect LWP and CF. The CDNC is prescribed as a constant value of 250 cm^{-3} in Morrison scheme for WRF-CMAQ and WRF-Chem or 300 cm^{-3} in Thompson scheme for WRF-CHIMERE without enabling aerosol feedbacks or ARI. The prognostic CDNC calculation is performed in WRF-Chem and WRF-CHIMERE with enabling ACI or both ARI and ACI by utilizing the maximum supersaturation (Abdul-Razzak and Ghan, 2002; Chapman et al., 2009; Tuccella et al., 2019).*" is added.

Lines 583-594: "*Such diversity in NMB variation can be explained by two aspect differences. First, model-top boundary conditions, for the WRF-CMAQ model, the potential impacts of stratosphere-troposphere O_3 exchange are considered via the parameterization of O_3-potential vorticity correlations (Xing et al., 2016) and used in our study, but not been in WRF-Chem (Grell et al., 2005). For the WRF-CHIMERE, climatological data or concentrations of coarse simulation can be used to represent model-top boundary conditions, and we applied the climatology from a general circulation model developed at the Laboratoire de Météorologie Dynamique (LMDz) coupling a global chemistry and aerosol model INteractions between Chemistry and Aerosols (INCA) (Mailler et al., 2017). Secondly, for gas-phase chemistry mechanisms, three coupled models incorporate a variety of photolytic reactions, with a more comprehensive explanation provided in Section 4.2.*" is added.

Line 691-699: "*More detailed interpretations were grouped into four aspects: (1) AODs are calculated via Mie theory using refractive indices of different numbers (5, 6 and 10) of aerosol species group in different coupled models (WRF-CMAQ, WRF-Chem and WRF-CHIMERE) (Tables S4 and S5); (2) 7 (294.6, 303.2, 310.0, 316.4, 333.1, 382.0 and 607.7 nm), 4 (300, 400, 600 and 999 nm), and 5 (200, 300, 400, 600, and 999 nm) effective wavelengths are used in calculating actinic fluxes and photolysis rates in Fast-JX photolysis modules of WRF-CMAQ, WRF-Chem and WRF-CHIMERE, respectively;(3) Different calculating methods of aerosol and cloud optical properties exist in the Fast-JX schemes of three coupled models (Tables S4-S6); (4) 77, 52 and 40 gas-phase species involve 218, 132, 120 gas-phase reactions in CB6, CBMZ and MELCHIOR2 mechanisms, respectively.*" is added.

We exchanged sequence of Sections 2.1 and 2.2 in the revised manuscript to improve the readability. Also, the comparisons of seasonal simulations and satellite observations in Section 4.2 are merge a paragraph and interpretations of mode diversities regarding simulated column variables are rephase a paragraph.

The added references are as follows.

Alapaty K, Herwehe J A, Otte T L, et al. Introducing subgrid-scale cloud feedbacks to radiation for regional meteorological and climate modeling[J]. Geophysical Research Letters, 2012, 39(24).

Archer-Nicholls S, Lowe D, Utembe S, et al. Gaseous chemistry and aerosol mechanism developments for version 3.5.1 of the online regional model, WRF-Chem[J]. Geoscientific Model Development, 2014, 7(6): 2557-2579.

Binkowski F S, Arunachalam S, Adelman Z, et al. Examining photolysis rates with a prototype online photolysis module in CMAQ[J]. Journal of Applied Meteorology and Climatology, 2007, 46(8): 1252-1256.

Binkowski F S, Roselle S J. Models-3 Community Multiscale Air Quality (CMAQ) model aerosol component 1. Model description[J]. Journal of geophysical research: Atmospheres, 2003, 108(D6).

Chapman E G, Gustafson Jr W I, Easter R C, et al. Coupling aerosol-cloud-radiative processes in the WRF-Chem model: Investigating the radiative impact of elevated point sources[J]. Atmospheric Chemistry and Physics, 2009, 9(3): 945-964.

Fu Q. An accurate parameterization of the solar radiative properties of cirrus clouds for climate models[J]. Journal of climate, 1996, 9(9): 2058-2082.

Grell G A, Freitas S R. A scale and aerosol aware stochastic convective parameterization for weather and air quality modeling[J]. Atmospheric Chemistry and Physics, 2014, 14(10): 5233-5250.

Heymsfield A J, Matrosov S, Baum B. Ice water path–optical depth relationships for cirrus and deep stratiform ice cloud layers[J]. Journal of Applied Meteorology and Climatology, 2003, 42(10): 1369-1390.

Hong S Y, Juang H M H, Zhao Q. Implementation of prognostic cloud scheme for a regional spectral model[J]. Monthly weather review, 1998, 126(10): 2621-2639.

Hu Y X, Stamnes K. An accurate parameterization of the radiative properties of water clouds suitable for use in climate models[J]. Journal of climate, 1993, 6(4): 728-742.

Iacono M J, Delamere J S, Mlawer E J, et al. Radiative forcing by long-lived greenhouse gases: Calculations with the AER radiative transfer models[J]. Journal of Geophysical Research: Atmospheres, 2008, 113(D13).

Mailler S, Menut L, Khvorostyanov D, et al. CHIMERE-2017: From urban to hemispheric chemistry-transport modeling[J]. Geoscientific Model Development, 2017, 10(6): 2397-2423.

Menut L, Bessagnet B, Khvorostyanov D, et al. CHIMERE 2013: a model for regional atmospheric composition modelling[J]. Geoscientific model development, 2013, 6(4): 981-1028.

Menut L, Siour G, Mailler S, et al. Observations and regional modeling of aerosol optical properties, speciation and size distribution over Northern Africa and western Europe[J]. Atmospheric Chemistry and Physics, 2016, 16(20): 12961-12982.

Mocko D M, Cotton W R. Evaluation of fractional cloudiness parameterizations for use in a mesoscale model[J]. Journal of Atmospheric Sciences, 1995, 52(16): 2884-2901.

Pincus R, Barker H W, Morcrette J J. A fast, flexible, approximate technique for computing radiative transfer in inhomogeneous cloud fields[J]. Journal of Geophysical Research: Atmospheres, 2003, 108(D13).

Safieddine S, Boynard A, Coheur P F, et al. Summertime tropospheric ozone assessment over the Mediterranean region using the thermal infrared IASI/MetOp sounder and the WRF-Chem model[J]. Atmospheric chemistry and physics, 2014, 14(18): 10119-10131.

Wild O, Zhu X I N, Prather M J. Fast-J: Accurate simulation of in-and below-cloud photolysis in tropospheric chemical models[J]. Journal of Atmospheric Chemistry, 2000, 37: 245-282.

Xing J, Mathur R, Pleim J, et al. Representing the effects of stratosphere–troposphere exchange on 3-D O_3 distributions in chemistry transport models using a potential vorticity-based parameterization[J]. Atmospheric Chemistry and Physics, 2016, 16(17): 10865-10877.

Zaveri R A, Easter R C, Fast J D, et al. Model for simulating aerosol interactions and chemistry (MOSAIC)[J]. Journal of Geophysical Research: Atmospheres, 2008, 113(D13).